



Contents lists available at ScienceDirect

# Engineering Science and Technology, an International Journal

journal homepage: [www.elsevier.com/locate/jestch](http://www.elsevier.com/locate/jestch)



## The influence of cutting edge microgeometry on the broaching of Inconel 718 slots



Cristian Fabián Pérez-Salinas <sup>a,c,\*</sup>, Pablo Fernández-Lucio <sup>a</sup>, Ander del Olmo <sup>b</sup>,  
Iñigo Aldekoa-Gallarza <sup>b</sup>, Luis Norberto López de Lacalle <sup>a,b</sup>

<sup>a</sup> Dept of Mechanical Engineering, ESI Bilbao, University of the Basque Country, Alameda de Urquijo s/n, 48013 Bilbao, Spain

<sup>b</sup> Advanced Manufacturing Centre (CFAA), University of the Basque Country (UPV/EHU), Bizkaia Technology Park -Ed.202, 480170, Zamudio, Spain

<sup>c</sup> Universidad Técnica de Ambato, Faculty of Civil and Mechanical Engineering, Ambato, Ecuador

### ARTICLE INFO

#### Keywords:

Broaching process  
Process forces  
Flank wear  
Cutting edge preparation  
Friction phenomena

### ABSTRACT

In aero-engine production, the dovetails (firtrees) of turbine discs are manufactured by broaching. Introducing innovative micro-geometry modifications to broaching tools can significantly influence cutting force, energy consumption, tool wear, and cutting edge temperature during broaching. Therefore, this study aims to study this influence by treating the cutting edge by brushing with ceramic bristles. The results reveal that the increase in cutting edge radius significantly influences the cutting force, particularly its component in the forward direction, equating it to the tangential component. Furthermore, during the experimental tests, considerable wear was observed on the cutting edge, which generated strong vibrations detected through the force signals, accounting to poor surface quality and a higher coefficient of friction close to 1. The 2D simulations generated information on temperature distribution along the cutting edge profile. On the other hand, was observed the presence of subsurface damage characterized by distorted grain boundaries aligned with the cutting direction, along with the formation of uninterrupted non-serrated chips due to thermoplastic deformation. Further, 12 µm cutting edge radius exhibits the best performance in terms of cutting force, temperature, and surface quality.

### 1. Introduction

Machining is one of the fundamental processes in the production of critical components for automotive and aerospace industries. Despite the emergence of new manufacturing technologies, broaching remains the most reliable and precise process for many applications because of its simultaneous productivity and precision [1]. The broaching process involves significant costs, so the main objective is to minimize the force applied, the temperature generated, tool wear and the risk of damaging the surface of the workpiece.

Broaching is the only one certified for manufacturing aero-engine dovetail slots, usually known as a firtree due to its specific shape [2,3]. Firtree-shaped unique slots (Fig. 1c) require high precision (under 5 µm on pressure surfaces) and surface finish quality to optimize their functionality and prevent the initiation and propagation of cracks. Blades are held in place by a perfect fitting. Broaching tools have a large length; thus, several segments are mounted in a row, making them expensive and delicate to manufacture (Fig. 1a). The three sections of a broaching tool are roughing, semi-finishing, and finishing (Fig. 1b). For

roughing, broaching tools are made of sintered carbide. They are usually mounted in steel tool holders with simple rectangular sections, while for semi-finishing and finishing with the firtree shapes, tools are made of HSS (high-speed steel).

In the broaching process, the cutting force involves a) a tangential component in the direction of the cutting speed and b) thrust force in the perpendicular direction. The behavior of these force components varies depending on several factors, such as cutting conditions, material properties, tool geometry, and material [1].

#### 1.1. Challenges in machining Inconel 718 with rounded cutting edge

Owing to the diverse range of profiles found in broaching tools, there is a corresponding variation in cutting forces [4]. To gain a deeper insight into the effects of the cutting process, several researchers performed experimentation and simulation of cutting forces using a single profile, i.e., cutting with a single tooth [5–7]. Further it has been reported that the cutting tool geometry significantly influenced the cutting forces [6,8]. Moreover, the tool wear changes geometry and micro geometry, which can affect the cutting process in force and temperature.

\* Corresponding author.

E-mail address: [cperez072@ikasle.ehu.eus](mailto:cperez072@ikasle.ehu.eus) (C. Fabián Pérez-Salinas).

Nomenclature		
$v_c$	Cutting speed [m/min], in broaching - tool stroke movement.	$K_c$ Specific cutting force parameter [ $\text{N}/\text{mm}^2$ ]
$RPT$	Rise per tooth [ $\mu\text{m}$ ], it is equivalent to feed in turning	$VB_B$ Average flank wear land width
$r_\beta$	Cutting edge radius [ $\mu\text{m}$ ]	$Ra, Rz$ Profile measurements surface roughness [ $\mu\text{m}$ ]
$RPT/r_\beta$	Shape ratio	$\mu_m$ Merchant's theoretical coefficient of friction
$\alpha$	Cutting edge relief angle [ $^\circ$ ]	$\mu_a$ Albrecht's theoretical coefficient of friction
$\gamma$	Rake angle [ $^\circ$ ]	$S_\alpha$ Cutting edge segment on flank face [ $\mu\text{m}$ ]
$F_x, F_y$	Orthogonal cutting force components [N]	$S_\gamma$ Cutting edge segment on rake face [ $\mu\text{m}$ ]
$F_c$	tangential force [N].	$K$ Relationship determining the edge profile trend.
$F_f$	Feed force [N].	$FEM$ Finite Element Method
$P$	Plowing force [N]	$WEDM$ Wire Electrical Discharge Machining
$Q$	Chip-forming force [N]	$\varepsilon$ Infrared IR Emissivity
		$T_m$ Edge preparation time
		$lc$ Cutting length

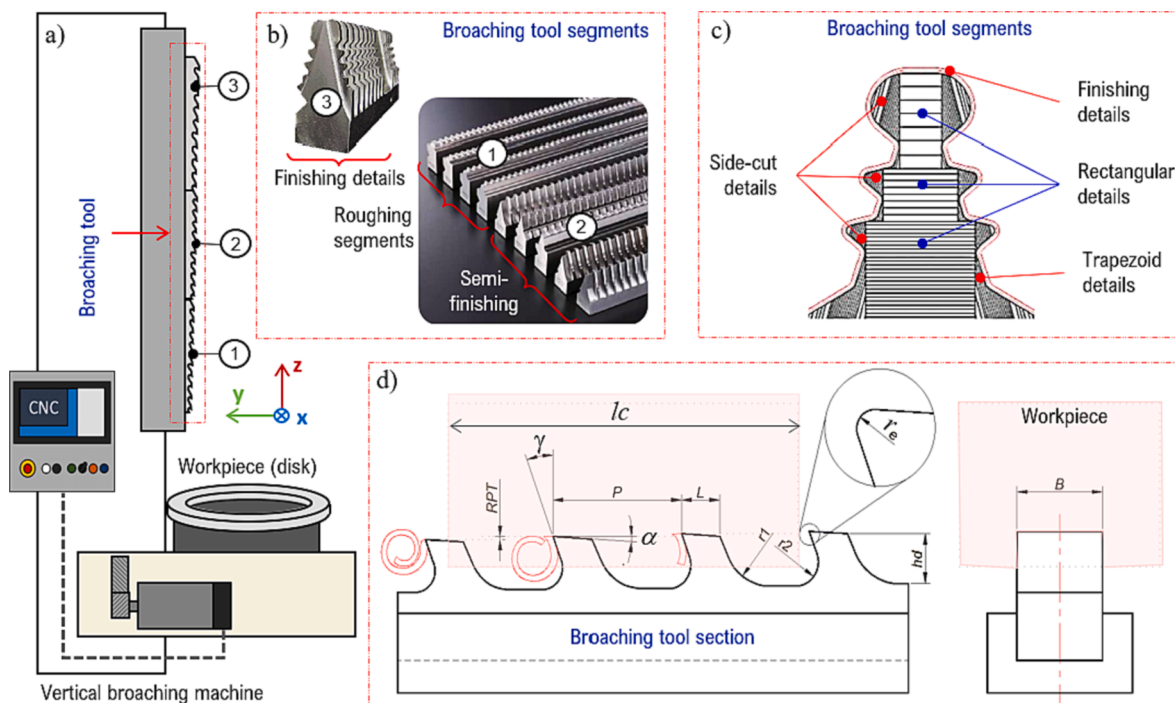


**Fig. 1.** Broaching process, a) Vertical broaching machine architecture, b) Broaching tool segments, c) Slot - firtree profile, d) Nomenclature of broaching tool parameters.

Researchers such as Grzesik et al. [9] and Arrazola et al. [10] provided experimental data showing the influence of wear on cutting forces.

One direct effect of the tool wear is the increase in temperature. Simulation techniques allowed researchers to learn about difficult-to-measure variables such as cutting temperature. Several researchers studied the behavior of cutting forces and temperature during the broaching process using 2D simulations. In this regard, Vogtel et al. [6] reported changes in cutting force and temperature in response to variations in the rake angle and cutting speeds. However, there is limited research regarding the impact of cutting-edge radius (microgeometry) on these variables. This aspect was explored in works such as [11,12] for milling and turning operations, respectively, where sensitivity analyses, simulations, and high-speed experiments have corroborated the significant effect. Even Rodriguez et al. [13] tested the influence of cutting edge radius after drag-finishing polishing before applying coatings. They further concluded that the coating technique is strongly affected by both the pre and post-cutting edge treatment.

Several works revealed the low quality of the machined surface as tool edge wear increases [1,14,15]. Thus, Alammari et al. [14] found that when machining heat-resistant alloys like Inconel 718, wear occurred on both the clearance and rake faces due to abrasive and adhesive wear. The same behavior was observed during the machining parts obtained by additive manufacturing of Inconel 718, but with a lower wear rate (30–40 %) than forged Inconel [16]. It was also found that a percentage error of around 20 % contributed to the Ra variability, where such error was attributed to the development of tool wear and rounding that were not considered [1]. Therefore, as the information on the effect of cutting edge radius and wear on surface quality is scarce, it is convenient to deepen the impact of these variables on Ra during the broaching of Inconel 718.

The quantitative determination of the coefficient of friction has received significant dedication in the scientific community. This enhanced interest is due to the friction affecting parameters like contact pressure, temperature, and sliding velocity occurring in a very small

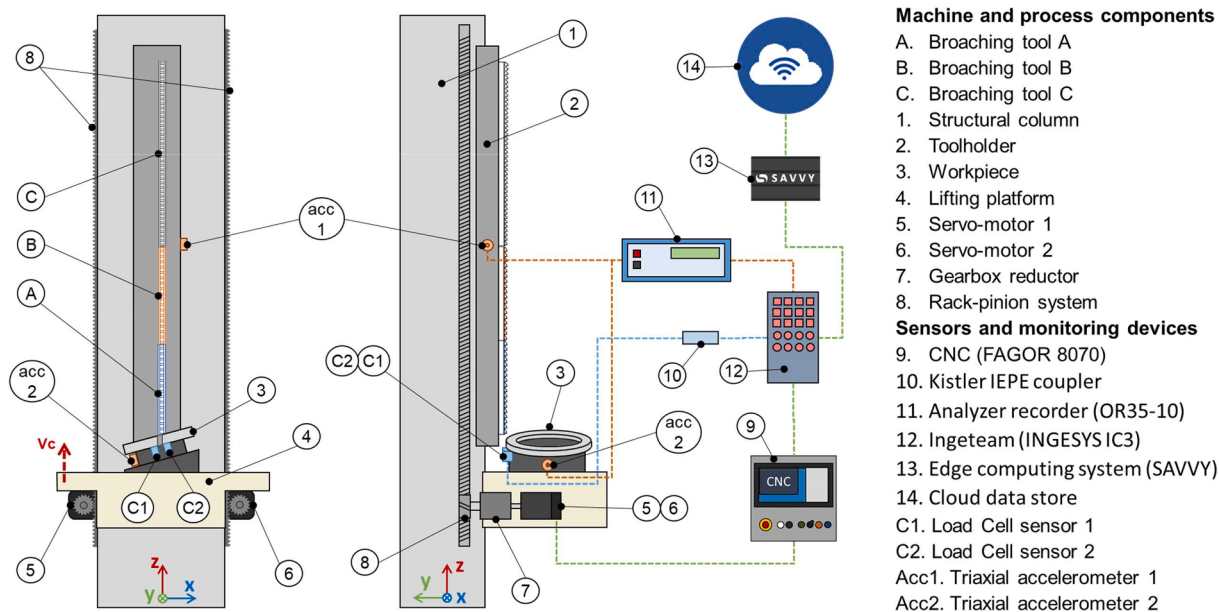


**Fig. 2.** Data acquisitions system architecture, which position of components, sensors devices of edge computing devices. Motor and rack pinion are twin, placed at both sides of the column [3].

area and for short intervals (10–3 s). Therefore, researchers developed different models that utilized various techniques and approaches, including analytical, experimental, and modeling [17,18]. Each model applies to different cutting processes and conditions involving many variables. From the cutting geometry perspective, the variables with the greatest impact on cutting forces are rake angle, depth of cut, and cutting edge radius [19,20]. Let's consider the depth of cut/cutting edge radius ratio (in broaching, it would be  $RPT/r_p$ ) as shown in Fig. 6. When the index exceeds 1, the effects around the cutting-edge radius are not considered significant. Conversely, when the index is close to or less than 1, the effects in the zone of incidence of the cutting edge radius can no longer be neglected.

Works, such as those by Childs [21] and Jaspers [22] experimentally verified the Zorev shear stress distribution [23], which divides the tool-chip contact into two zones: the adhesion and the sliding friction zones, each with their respective friction coefficients. Grzesik [24] also showed analytically that the apparent coefficient of friction consists of an adhesion component and a deformation component. Furthermore, considering the practical importance from an engineering standpoint, the reality facing broaching component manufacturers is that friction is not only in the tool-chip interaction. It also occurs in the tool-workpiece interaction and is present dynamically around the cutting edge radius [10]. Therefore, all these interactions directly affect chip formation, tool life, surface quality and process energy consumption, respectively.

In machining, the coefficient of friction in the tool-workpiece interaction is directly related. The coefficient of friction increases as the flank wear rate increases [4]. Works like [22] focused on determining the friction in the presence of flank wear during the machining of titanium Ti-6Al-4 V and nickel-based IN-100 alloys. This work concluded that the coefficient of friction differs with the change in workpiece material and slightly with the leading-edge geometry. However, the reported results are limited to cutting edge radii of 10 and 25  $\mu\text{m}$  and rake angles of 0 and 3°.

If the friction phenomenon at the cutting edge is considerable, changes in the controlled forces will occur. In broaching, the cut or uncut chip thickness (RPT) depth is close to the dimensions used in the finishing process in turning or milling (20–80  $\mu\text{m}$ ). If we add to this that if we increase the cutting radius at the cutting edge (10–40  $\mu\text{m}$ ), the  $RPT/r_p$  shape ratio will be close to or less than 1. Therefore, the friction phenomenon will increase and will be reflected in increases in the

cutting force components. Fang and Arrazola [10,25], reported on this behavior of the cutting force components and observed that machining Inconel 718 resulted in an increase in cutting force due to the wear of the rounded cutting edges.

### 1.2. Goal and significance of the present study

Del Olmo et al. [3] presented a full monitoring approach for the broaching process of aero engines using roughing rectangular shape broaching tools, using a machine shown in Fig. 2. The approach showed a direct influence of tool wear on cutting forces and power consumption. Still, the broaching bench didn't have sensor resolution enough to detect the effect of cutting edge radius on the process, and 3–4 teeth were cut simultaneously. Load cells C1 and C2 offer reasonable trend evolution data but could not provide a good cutting force value. Therefore, the work presented here will use a similarity model, a lathe, and a single tooth broaching tool section (Fig. 5).

Investigating manufacturing variables related to tool precision and quality is crucial to meeting the requirements of aeronautical components. Therefore, in this work, the effects of varying broaching radius on cutting forces, wear, and temperature in the broaching process of Inconel 718 are studied. Four different types of radii to the original broaching radius are examined and combined with three uncut cutting thicknesses (RPT) to determine their influence on the cutting process.

## 2. Experimental procedure

This section provides a detailed description of the following aspects: characterization of the cutting edge, the experimental setup utilized for testing, and the procedure for finite element modeling, employing a simplified approach of orthogonal cut.

### 2.1. Cutting edge radius characterization

Hence, from a rough broaching tool, segments of 20 to 30 teeth (Fig. 1b), single-edged broach sections were cut by WEDM, to perform a polishing process by brushing. The objective was to obtain cutting edge radius between 5 and 35 mm. Wire brushes with Xebect<sup>TM</sup> ceramic wire performed rounding of the cutting edges. The brushing tool was mounted on a three-axis CNC machine to ensure a controlled polishing

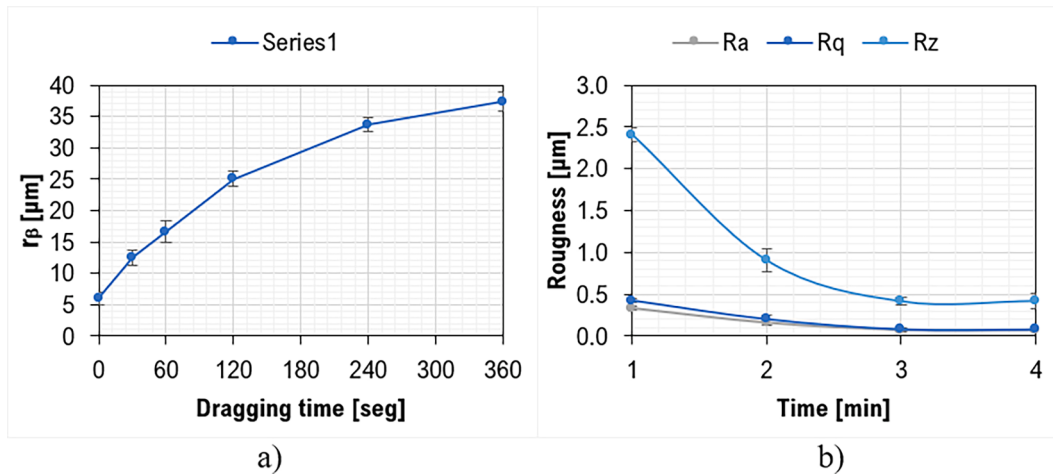


Fig. 3. Ceramic Bristle Brush Polishing Performance on sintered tungsten carbide.

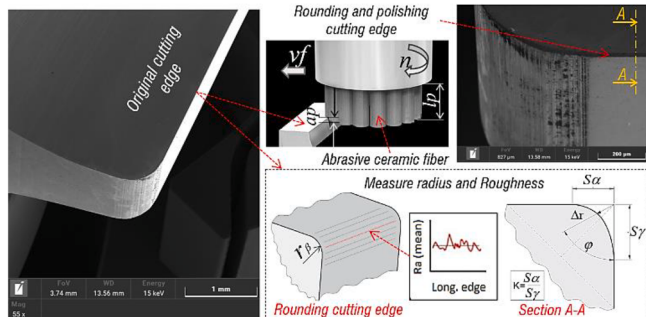


Fig. 4. Installation of experimental tests. left) original cutting edge, center) polishing brush, right down) cutting edge polished and Alicona™ measurements.

operation. Preliminary tests showed polishing performance (roughness  $R_a$ ,  $R_p$ ,  $R_z$ ) and cutting-edge rounding ( $r_p$ ) on uncoated tungsten carbide broaches (Fig. 3).

According to Fig. 3, it took 6 min of polishing to achieve a radius of 37 μm, while reducing the lower roughness achievable with this type of

brush took 3 min. In these brushes, the process pressure is determined by the combined length of the wire protruding from the outer cylinder,  $l_p$ , and the depth to which the brush bristles are introduced over the cutting edge as the brush rotates,  $a_p$  (see to Fig. 4). The cutting-edge rounding was characterized using the method proposed by Denkena et al. [26]. The edge measuring instrument was an Alicona™ Infinite Focus, as shown in Fig. 1.

## 2.2. Experimental setup

Our previous work [3] explains that broaching tracking on hydraulic or electromechanical machines and benches is quite complex. Therefore, to characterize the cutting edge, an equivalent arrangement for broaching with a tooth on a turning center with a capacity of 5000 N in all three axes was proposed (see Fig. 5). Feed motion about the X-axis of the lathe was used to mimic the broaching cutting motion. The cutting speed for the broaching process was limited by the feed rate capability of the machine, which ranged from 0 to 30 m/min. Therefore, a broaching cutting speed of 20 m/min was selected, as it is in the usual range of cutting speeds in the rough broaching process. The mounted workpiece was a nickel-based superalloy (WNR 2.4668/aged Inconel 718/45 HRC) 100 mm diameter by 70 mm long, resulting in a cut length of 70 mm for

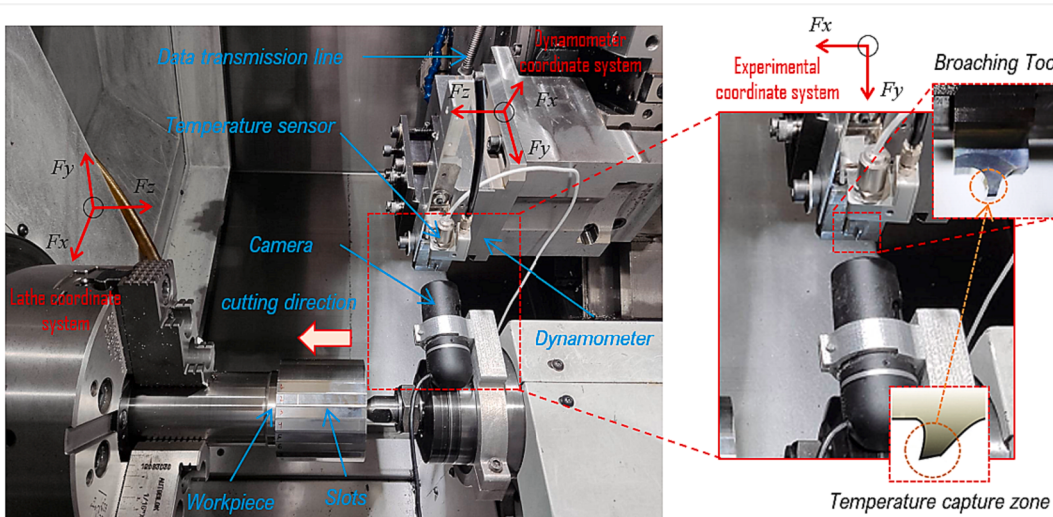


Fig. 5. Installation of experimental tests.

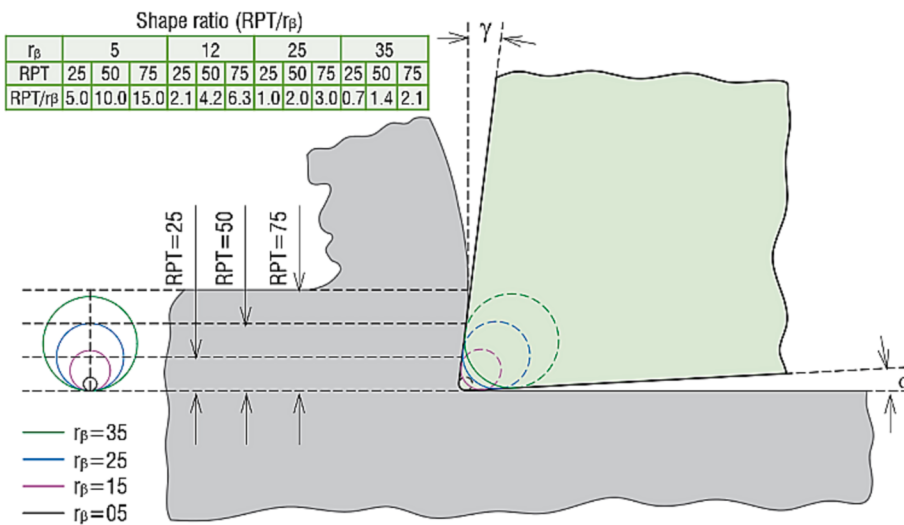


Fig. 6. Shape ratio at cutting edge used in the experiment.

**Table 1**  
Factors levels for experimental application.

Parameter	Symbol	Unit	Value
Cutting speed	$v_c$	(m/min)	20
Rake angle	$\gamma$	(°)	7
Clearance angle	$\alpha$	(°)	3
cutting width	B	(mm)	8
Rise per tooth	RPT	( $\mu\text{m}$ )	25, 50, 75
Radius edge	$r_\beta$	( $\mu\text{m}$ )	5, 12, 25, 35

all cuts made. The stiffness of the machine is well known [27] and provides excellent rigidity, minimizing vibrations. All orthogonal broaching experiments were performed under dry conditions. The tool used in the experiments was an uncoated sub-micro grain tungsten carbide tool with a 6 %Co composition and an 8 mm cutting width.

Table 1 summarizes the tool geometry and cutting parameters employed in the tests. It is important to emphasize that the  $RPT$  variation was selected according to the usual ranges for the IN718 broaching roughing process. The cutting-edge radius is used from the original 5  $\mu\text{m}$  to an increment of 35  $\mu\text{m}$  to analyze its effect on the control variables. Fig. 6 illustrates the “shape index,” which relates the uncut chip thickness  $RPT$  to the cutting edge radius  $r_\beta$  used in the experiment.

### 2.3. Measurement of response variables

Cutting force was measured using a Kistler force dynamometer under orthogonal cutting conditions, with a measuring range of  $\pm 10$  kN in the z-axis and  $\pm 5$  kN in the x- and y-directions. Two repetitions were performed for each broaching state, and a third repetition was performed if the standard deviation was larger than 7 %.

An OPTRIS™-CT-2 M infrared thermal camera with a 1 ms resolution was used to monitor the temperature on the tool's lateral cutting edge (see Fig. 5). The emissivity of tungsten carbide can vary depending on several factors, such as temperature and surface texture. In general, the emissivity of tungsten carbide is relatively low, with typical values ranging from 0.05 to 0.35 [28]. The contact method was employed for calibration of the infrared temperature sensor (IFS) [29], where the tool was heated to a reference temperature measured by contact with a calibrated thermocouple. The emissivity setting was changed until the actual tool temperature was measured with the IFS, with the obtained value of  $\epsilon = 0.248$ .

Microhardness was measured on the sample's cross-section in the cut's direction using the Vicker microhardness tester. The indentations

**Table 2**  
Constants of the Johnson cook equation.

A [MPa]	B [MPa]	C	n	m	$\bar{\epsilon}_0 (\text{s}^{-1})$	$T_r$ (°C)	$T_m$ (°C)
851.67	657.62	0.0105	0.2280	3.1169	1	20	1500

were made using a diamond dresser with an axial load of 50 gf for a dwell time of 15 s from a depth of 10 to 400  $\mu\text{m}$  from the machined surface.

To obtain the roughness profile ( $R_a$  and  $R_z$ ) and the profile of the worn cutting edge, an Alicona Infinite Focus confocal microscope was used to scan the area of interest. From the scan of the machined area, the arithmetic mean of the roughness profile ordinates,  $R_a$ , and the highest height of the roughness profile  $R_z$  are measured according to ISO 4287:1999 (Fig. 16). On the other hand, once the scan of the cutting edge zone was obtained, the flank wear length was measured and the wear profile was extracted (Fig. 12).

### 2.4. Finite element modelling

Orthogonal cutting was modelled using Deform™ 2D software package, which employs an implicit Lagrangian formulation. The model consisted of two distinct bodies - the tool and the workpiece. A cutting tool was defined solely as a rigid body, allowing only the work piece to deform. The workpiece was modelled with a rectangular cross-section of 4 x 1 mm and with a mesh comprising between 15 and 30 elements in the uncut chip thickness and between 3000 and 8000 isoperimetric quadrilateral elements with a unit aspect ratio, based on the specific requirements of the conditions. The tool, on the other hand, was modelled using meshing with 5000 elements, with a higher density in the tip area featuring elements that were 120 times smaller than those in the rest of the tool. Both cemented carbide and Inconel 718 thermal properties were obtained from the Deform 2D library. The constitutive equation of Inconel 718 was determined using the inverse method. The constants A, B, C, m, and n of the Johnson Cook equation (1) were identified according to Vogtel works [6], as shown in Table 2.

$$\sigma_{yld} = [A + B \cdot \dot{\epsilon}^n] \cdot \left[ 1 + \ln \left( \frac{\dot{\epsilon}}{\dot{\epsilon}_0} \right) \right] \cdot \left[ 1 - \left( \frac{T - T_0}{T_{melt} - T_0} \right)^m \right] \quad (1)$$

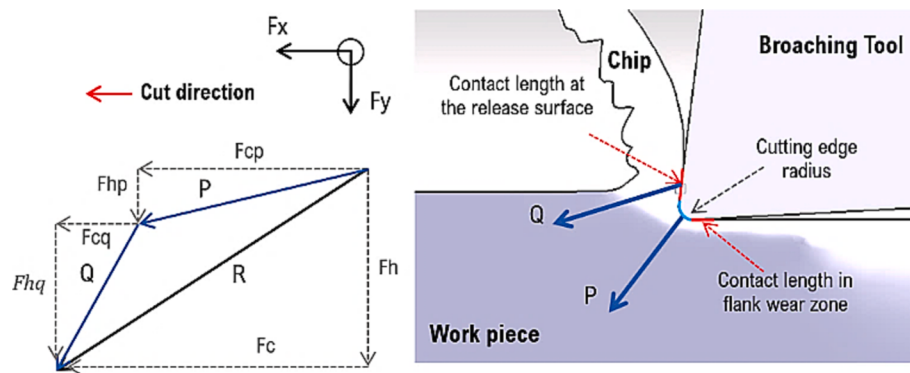


Fig. 7. Characterization of the honed cutting edge.

### 2.5. Friction and wear analysis

The high friction during machining processes has a notable influence on heat concentration, leading to elevated tool wear. This effect is evident in difficult-to-cut materials such as nickel-based alloys, which possess low thermal conductivity and exhibit chemical affinity with tool materials at high temperatures. Consequently, the integrity of machined surfaces can be compromised.

Numerous attempts have been made to determine friction during machining, but this is a complex task due to the various phenomena involved in the workpiece-cutting tool interaction in the cutting operation. In their study, Ulutan and Özcel [15] showcased how stress distribution is affected by the cumulative friction experienced across the cutting-edge geometry. The cutting geometry includes the profiles of the cutting surface, the cutting edge, and the incidence surface. Zorev [30] proposed quasi-stationary friction and an average friction coefficient value, while Arrazola et al. [10], showed that the friction coefficient is not constant and recommended a variable friction coefficient empirically obtained from cutting tests. Furthermore, the authors showed that rake angle, clearance angle, and uncut chip thickness are parameters affecting friction.

Two practical simplifications can help to understand the magnitude of friction during the cutting process. The first equation makes it possible to obtain a constant average friction coefficient ( $\mu_m$ ) proposed by Merchant (Equation (2) [31]). On the contrary, the Albrecht method allows measuring the coefficient of friction of the tool-chip surface by eliminating the effects of the cutting edge (Equation (3) [32]). The two equations are approximations to find the Coulomb coefficient of friction by experimental tests.

$$\mu_m = \operatorname{tg} \left[ \operatorname{arctg} \left( \frac{F_y}{F_x} \right) + \gamma \right] \quad (2)$$

$$\mu_a = \frac{\sin \gamma \cdot F_h c + \cos \gamma \cdot F_h f}{\cos \gamma \cdot F_h c - \sin \gamma \cdot F_h f} \quad (3)$$

According to Albrecht orthogonal cutting scheme [32], the shear force  $R$ , resulting from the measured forces ( $F_f$ ) and ( $F_c$ ) feed and tangential forces, respectively, can also be decomposed into two forces,  $P$  and  $Q$ , called ploughing force and chip-forming force (Fig. 7). An important point of Albrecht model is that it separates the shearing effect from the ploughing effect. The ploughing effect is important when the friction phenomenon is considerable at the cutting edge.

To evaluate the wear of turning tools, the machining literature focuses on the average flank wear land width  $VB_B$ , and crater depth  $KT$ .  $VB_B$  and  $KT$  are designations according to ISO 3685 of 1993. However,  $VB_B$  is often used to monitor tool wear because of the relative ease of its measurement.  $VB_B$  is measured at the parting face of the cutting tool [25]. The wear phenomenon does not develop independently but is closely related to several factors, such as surface sharpness, surface quality, and micro-geometry. When we talk about tool surface sharpness, it is influenced by the presence of small chips or microchips generated during the cutting edge manufacturing process, which affect the wear of the tool (Fig. 8). Finally, it has been shown that achieving the correct microgeometry and roughness on the cutting edge can significantly impact extending tool life.

In the aircraft industry, edge wear is an indicator of whether a tool is suitable for component manufacture, with a usual value of around  $20 \mu\text{m}$  ( $30 \mu\text{m}$  is recommended by ISO standard). Another reason for the use of

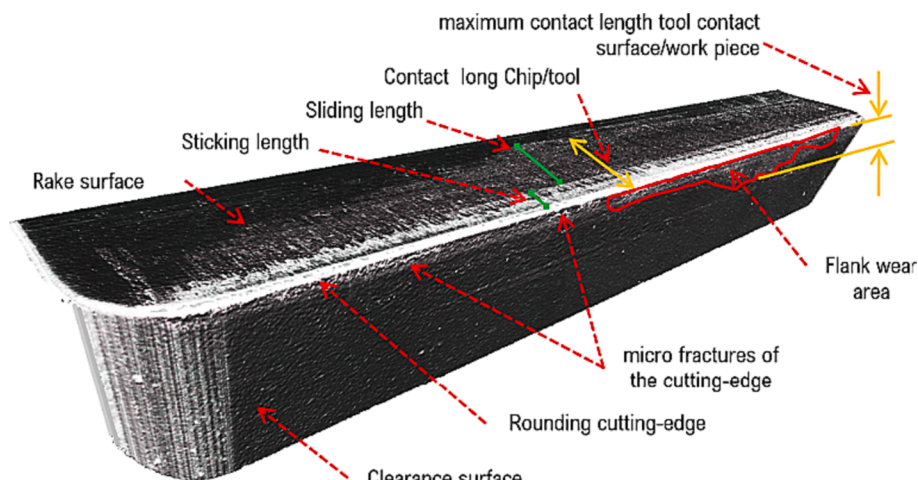


Fig. 8. Characterization of the cutting edge of worn brushes. Images acquired by three-dimensional scanning of surfaces with confocal microscopes.

**Table 3**  
Cutting edge rounding characterization results.

Conditions	$r_p$ [μm]	K	* $T_m$ [min]	$R_a$ [μm]	$R_z$ [μm]
Original	5 +/- 1.5	1.45	0	0.226	1.121
Rounding 1	12 +/- 1.2	1.31	60	0.198	1.234
Rounding 2	25 +/- 1.0	1.03	130	0.079	0.528
Rounding 3	35 +/- 1.0	1.18	300	0.085	0.438

\* Edge preparation time by brushing.

flank wear is that its location makes it more easily accessible due to the geometry of the tool and the arrangement of the cutting system, such as on broaching machines.

### 3. Results and discussion

This section details the results of cutting edge preparation, process force components, temperature in the lateral zone of the tool cutting edge, and friction behavior and tool wear under process control variables.

#### 3.1. Rounding and polishing of cutting edges

The cutting edges of the broaches to be used for the test were prepared and characterized. Table 3 shows the results obtained. Overall, the data tended to symmetrical rounding with  $K$  values close to 1, indicating total symmetry. The original manufacturing rounding was approximately 5 μm before the cutting edge was polished. After a preparation

time of  $T_m$ , cutting edge radius of 15 μm, 25 μm, and 35 μm was achieved, which fall within the common ranges of broaching tool manufacture and the favorable results found in previous research on machining Inconel 718 [11,33,34]. Moreover, the results demonstrated that as the planning time  $T_m$  increased, the radius obtained also increased, while the average roughness of the cutting edge decreased. It is worth noting that due to the nature of the contact between brush bristles and cutting edge, this preparation technology has limitations in controlling the microform variation and symmetry/asymmetry.

#### 3.2. Effects on broaching process forces and temperature

Fig. 9 shows the results of the force measurements obtained by the dynamometer on the orthogonal cutting axes, where  $F_c$  is the cutting force component and  $F_f$  is the feed force component. The influence of the radius of the cutting edge and for each  $RPT$  on the forces can be seen in each of the figures. The sensitivity of the tangential force and the feed force to the change of the edge radius show similar intensity. This sensitivity is evidenced by an increase proportionally of the cutting edge radius. Furthermore, this proportional force increase is replicated as the uncut thickness changes. The tests indicate that the range of thrust forces  $F_f$  is like that of tangential forces  $F_c$ . This finding differs from other studies [15,35], which reported low values of  $F_f$  compared to  $F_c$  when machining titanium alloys. However, in the study of Ulutan and Özal [15],  $F_f$  was higher than  $F_c$  at an angle of attack  $\gamma = 0$ , and the forces were similar when  $\gamma = 3$  for machining Inconel. Therefore, this trend change in orthogonal machining of Inconel may be influenced by

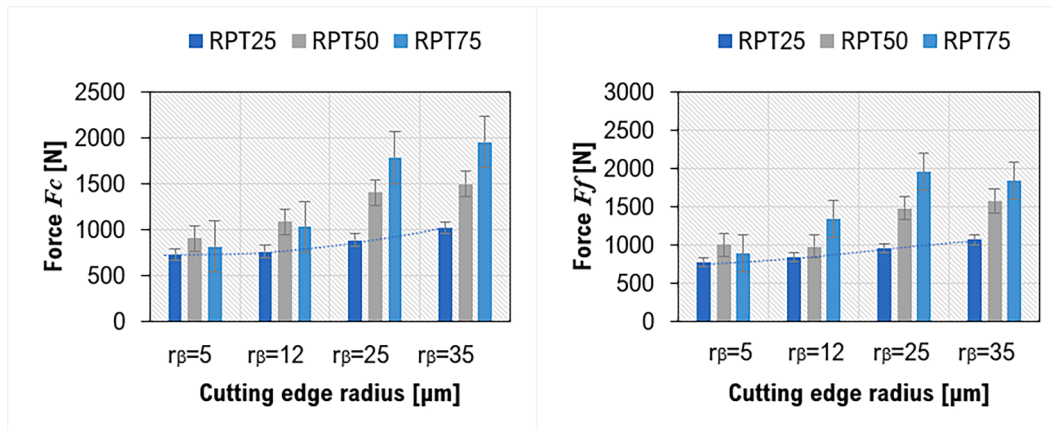


Fig. 9. Cutting force components generated by the machining process.

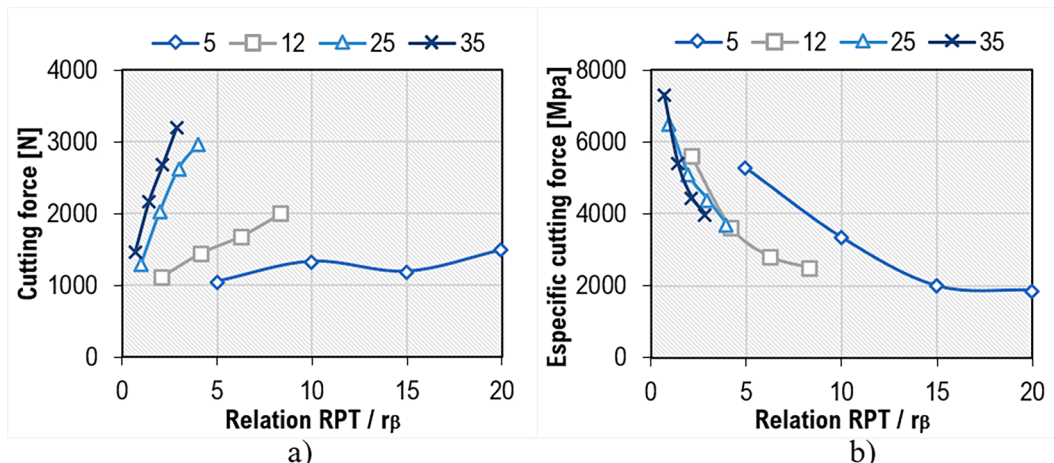
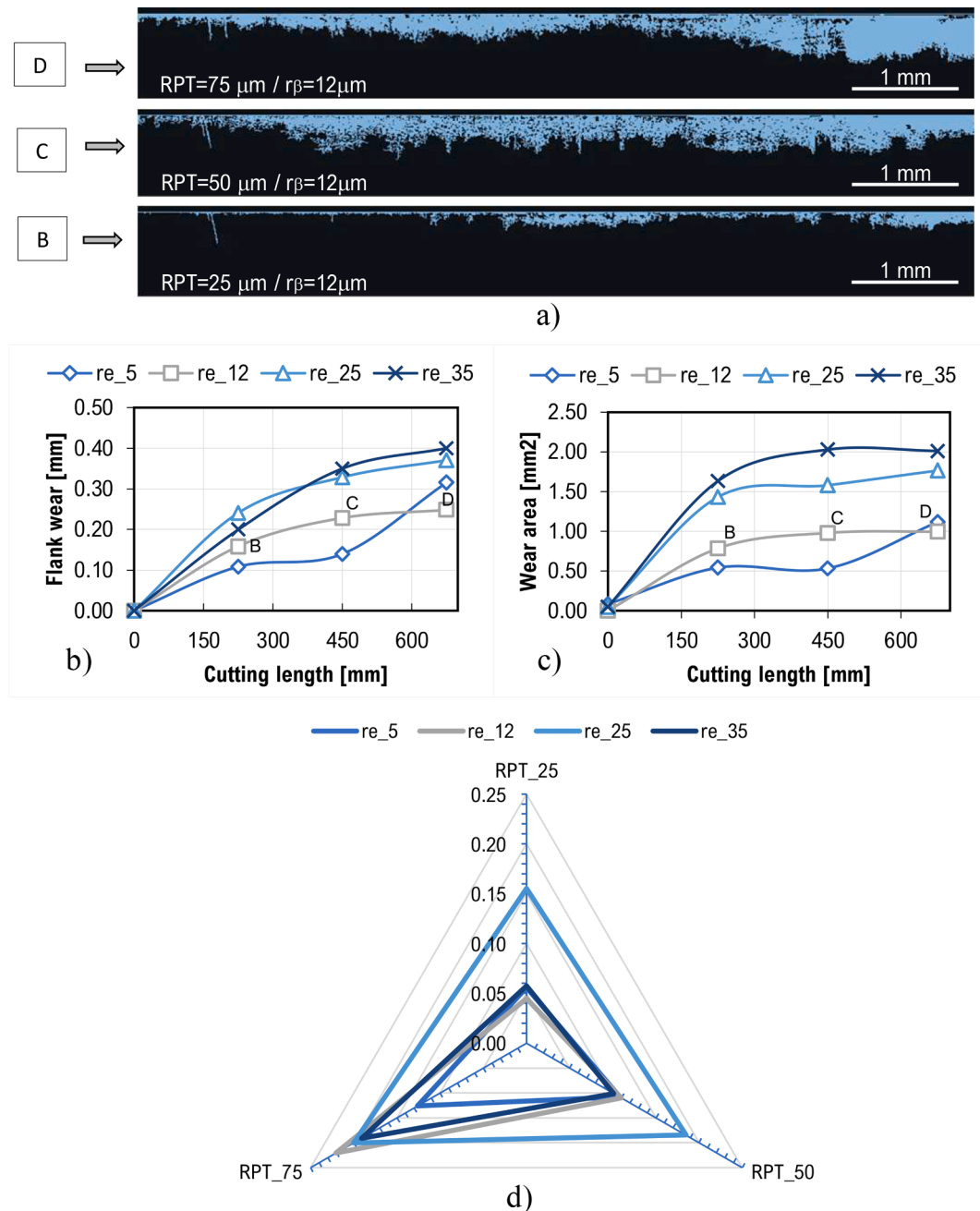


Fig. 10. Force and specific cutting force as a function of the relation  $RPT / r_p$ .



**Fig. 11.** Development of flank wear, a) detection by image processing measurement of the flank wear area, b) evolution with respect to cut length, Flank ear area vs cutting length, d) RPT influence.

other cutting conditions, such as flank wear and chip-tool contact length, among others, which need to be further clarified.

Fig. 10 shows the behavior of cutting force and specific cutting force about the aspect ratio ( $RPT/r_{\beta}$ ). When the aspect ratio is small, a significant increase in shear strength is observed, i.e., this tendency is present when the radius is large. On the contrary, the cutting force will be smaller when the aspect ratio is large, which is affected by a small radius. Therefore, this behavior found in the shear tests is presumed to be related to the so-called “plowing effect” in the cutting process.

The specific cutting force  $K_c$  refers to the force required to remove one unit area of material. In broaching, the specific cutting force varies as a function of the material type, cutting speed, feed rate, and tool geometry. Tests demonstrated the influence of micro geometry (cutting edge radius) on the specific cutting force, as shown in Fig. 10b. Studies on machining soft materials, such as those performed by Lucca [36,37]

and recently by Rahman [37], demonstrated that increasing the shape ratio can reduce  $K_c$ . This is due to the phenomenon of the “size effect,” where decreasing the shape index causes an increase in the effective rake angle, which in turn increases the specific cutting force, as reported by Sun and Cheng [38]. In the tests performed, this effect was also observed when machining Inconel, even in flank wear of 0.10 mm above the permissible value ( $VB_B = 0.2$  mm), as seen in Fig. 11b.

### 3.3. Friction and wear behavior in orthogonal broaching

Fig. 11 shows the evolution of flank wear when 10 grooves were made in Inconel 718, covering a total length of 700 mm. Due to the rectangular geometry of roughing broaches at the incidence surface, the area of flank wear in this region is highly visible. Fig. 11a illustrates the wear in the flank area using image processing, a technique commonly

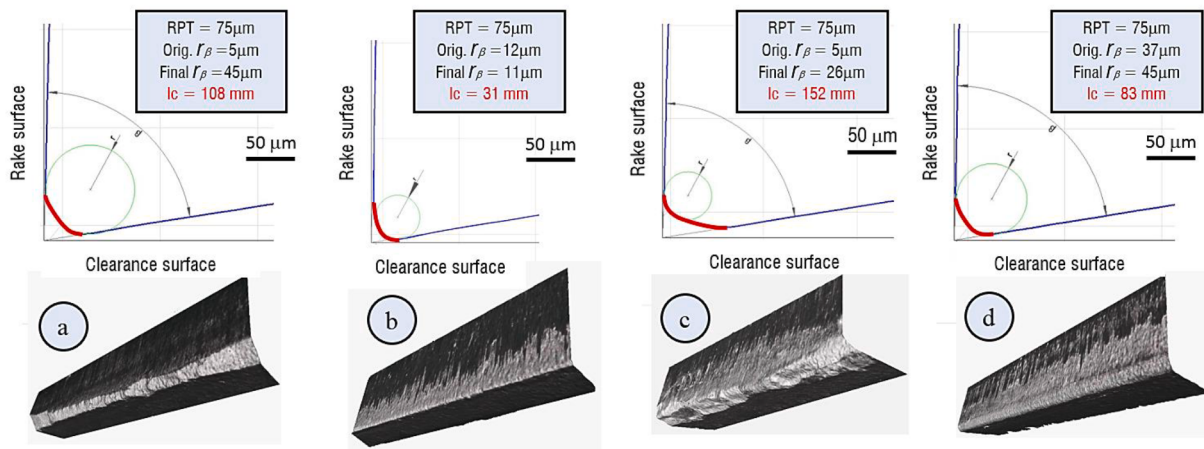


Fig. 12. Representative profiles of the broaching tool cutting edge after cutting process.

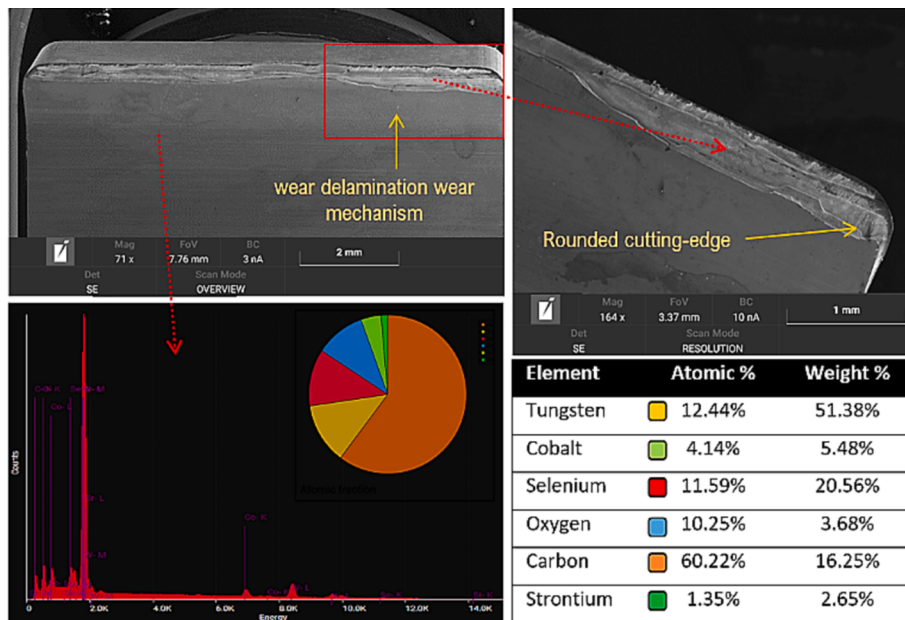


Fig. 13. SEM microscopy image of delamination wear on the cutting edge and chemical analysis by EDX spectroscopy of the tool material.

used to detect types of wear, including crater wear [39,40]. Previous works have also applied this method of flank wear measurement in broaching processes [41,42]. The wear area is determined by identifying the area of interest through image processing techniques and deducing it by pixel counting in the incidence area, then transforming it to standard surface units based on the corresponding scale. Although there is no specific standard for measuring flank wear in broaching processes, the standard (ISO 3685:1993) applicable to turning processes is used. Fig. 11b shows the flank wear  $VB_B$  results for the tested conditions and can be compared with the flank wear area results (Fig. 11c). Furthermore, flank wear  $VB_B$  steadily increases with increasing  $RPT$  for the 4 cutting edge radius tested (Fig. 11d). This is clearly illustrated in Fig. 11a for the 12  $\mu\text{m}$  cutting edge radius case.

The correlation between flank wear measured according to ISO 3685

and wear obtained by image processing was 89.5 %. Both show similar trends and curve fits, although they are measured in different units (area and length). Evaluating “wear per unit area” provides a more accurate representation of its actual dimension on the flank. Therefore, the wear area can be a useful metric for monitoring and evaluating flank wear progression. However, it is important to consider that the results depend on the resolution and sharpness of the images used in the processing.

The initial rounded cutting edges experienced wear in different degrees and shapes during testing. We observed microfractures at various locations along the tool edge, forming a bevel (Fig. 12a, 12c), asymmetric wear of the rounded cutting edge (Fig. 12b), and symmetric wear of the rounded cutting edge (Fig. 12d). These wear patterns have been reported in previous studies [25].

The cutting edge experienced a total collapse at a cutting length of 910 mm (after 12 broached slots), as shown in Fig. 13. This test was performed with  $RPT = 75 \mu\text{m}$ ,  $r_\beta = 25 \mu\text{m}$  and  $v_c = 20 \text{ m/min}$ . During the test, flank wear exceeded  $VB_B = 0.39 \text{ mm}$ . A delamination wear mechanism was observed along the entire length of the cutting edge. In addition, the figure shows the properties obtained from the elemental chemical analysis performed by EDX spectroscopy.

Using equations (1) and (2), the average friction coefficients at the

Table 4  
Average friction coefficients for each tested cutting edge radius.

$r_\beta$	5 $\mu\text{m}$	12 $\mu\text{m}$	25 $\mu\text{m}$	35 $\mu\text{m}$
$\mu_a$	0.683	0.808	0.793	0.925
$\mu_m$	1.046	1.217	1.248	1.390

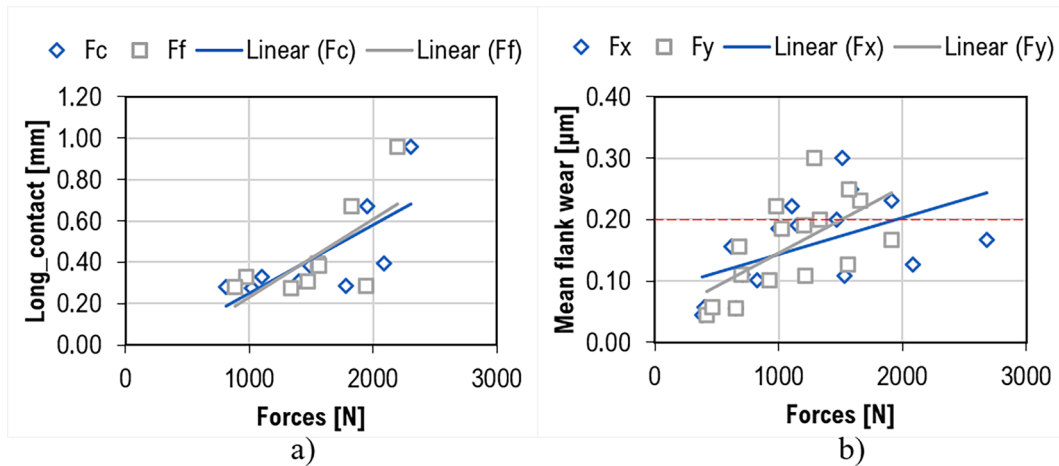


Fig. 14. Variation of broaching process forces in relation to a) chip-tool contact length, and b) flank wear  $VB_B$ .

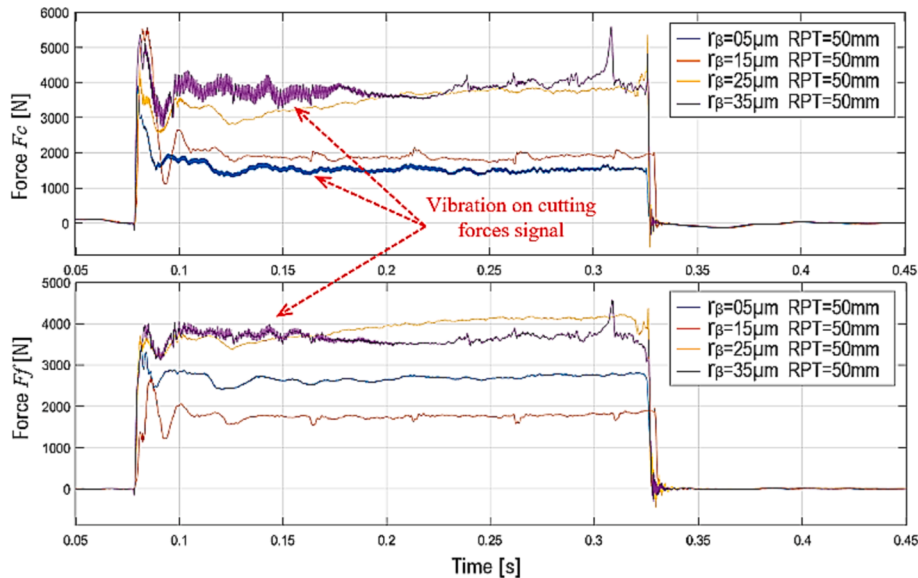


Fig. 15. Monitored forces of the orthogonal broaching process with  $v_c = 20 \text{ m/min}$  and  $RPT = 50 \mu\text{m}$ .

tool-chip interface with different cutting edge radii were determined and given in Table 4. It is observed that the values are in the range of 0.7 to 1.4 for broaching Inconel 718 under dry conditions. The coefficient of friction proposed by Merchant is higher than the coefficient of friction given by Albrecht. This is because Albrecht considers friction only on the rake surface without considering the effect of plowing and the rounded cutting edge profile. Therefore, comparing the two obtained values of the coefficient of friction would assume an existing contribution to friction from the cutting edge.

The above friction coefficient values  $\mu_a$  and  $\mu_m$  obtained in this study were higher compared to similar works, such as the study conducted by Alammari. et al., [14]. Based on observations, it is estimated that this difference in values can be attributed to two factors: the increase of the chip-tool contacts length and flank wear, as illustrated in Fig. 14a and 14b, respectively. These factors lead to an increase in the process forces  $F_c$  and  $F_f$ , which are involved in equations (1) and (2) of the coefficients of friction. Thus, resulting in higher values of the friction coefficient. It is important to note that while these factors may explain the difference in values, it is crucial to consider other potential factors that may have contributed to the observed results. For example, a tribological speculation given by [21] states that for friction coefficients greater than 1 to exist, there must be the strongest levels of adhesion between the

asperities and the tool. However, for the moment, no quantitative theory describes it accurately.

Another factor that can contribute to the increase in cutting force components, especially the feed force, is the growth of the cutting edge radius or contact length of the worn edge (Fig. 12). As the cutting edge wears, there is a noticeable increase in both the cutting edge radius and contact length in all the cases presented. This results in a slightly greater uncut chip thickness than the tool edge dimension, which causes friction. Instead of cutting, the tool tends to burnish the surface. Several research studies have shown that the  $F_f$  force can be as large as the  $F_c$  force [43–45]. Fig. 15 illustrates this phenomenon, displaying a noticeable alteration in the ratio of the  $F_f$  component in relation to  $F_c$  for each rounded edge. When the thrust force  $F_f$  increases, it can diminish the lifespan of the tool edge and give rise to vibration and damping effects during the interaction between the tool and the material. These consequences ultimately lead to a decline in surface quality.

Fig. 16 illustrates chip formation and Grain boundary deformation in the near-surface layer during the dry broaching process, using an RPT of 35  $\mu\text{m}$  for different cutting edge radii. In all cases, it is observed that plastic deformation was the predominant factor in chip formation, as shown in the micrograph of the chip (Fig. 16a). At the macroscopic level, the degree of rolled-up chips was variable. Total chip deformation

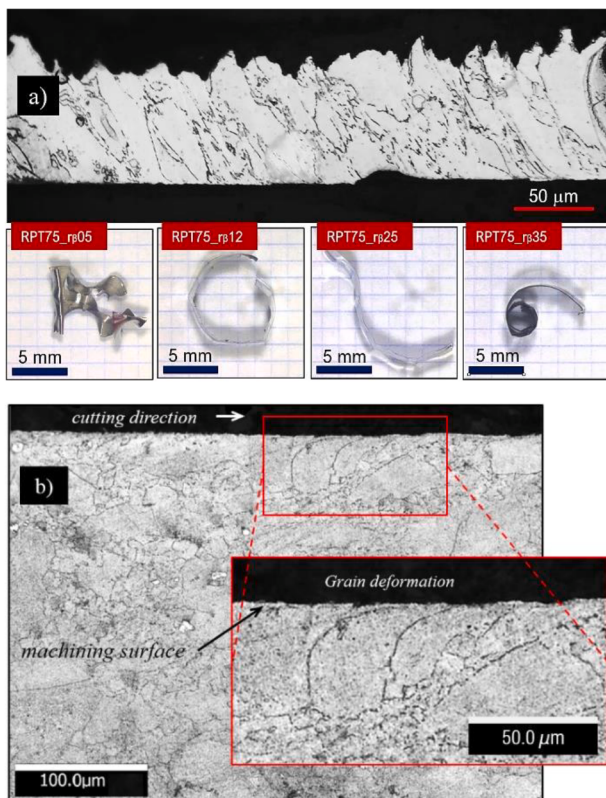


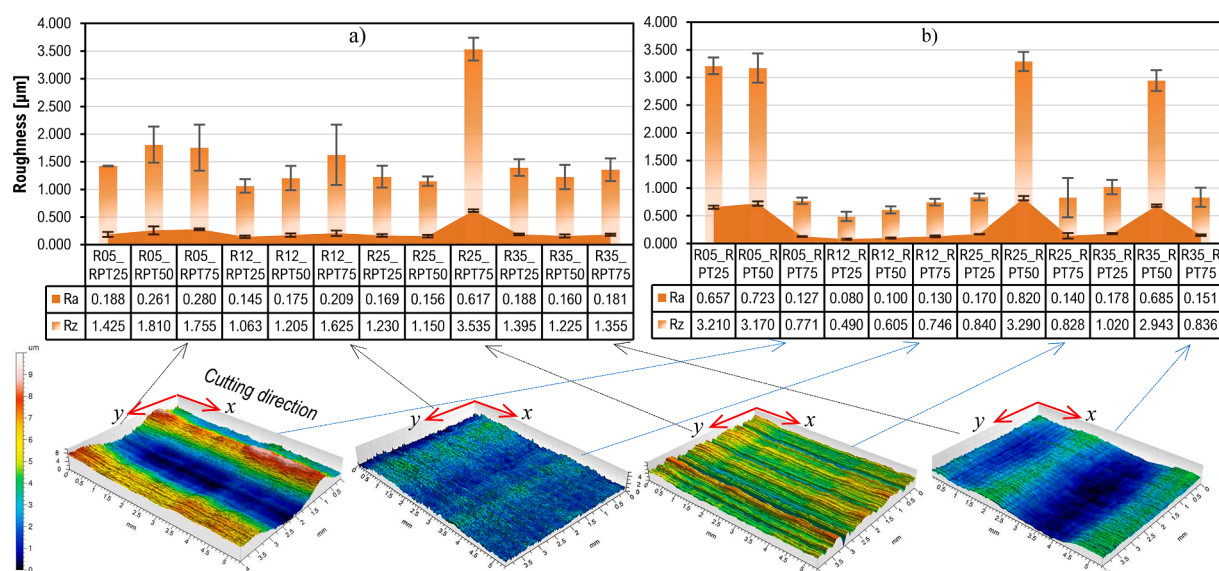
**Fig. 16.** A) Chip formation, comparison of different cutting edge radius in dry machining, b) Grain boundary deformation in the near Surface layer.

occurred when a cutting edge radius of 5  $\mu\text{m}$  was used. This could be attributed to wear and microfractures along the tool cutting edge that entrained and deformed the chip. For the case of the 25  $\mu\text{m}$  cutting edge radius, the cutting edge wear caused a re-sharpening of the cutting edge and an asymmetrically shaped beveled nose profile (Fig. 12a). The result was an elongated chip that exhibited winding. On the other hand, the drastic increase of the cutting edge radius to 35  $\mu\text{m}$  increased friction significantly. This presumably generated an increase in temperature in the primary zone, which produced a complete coiling of the chip. Finally, moderate deformation was observed in the case of the 12  $\mu\text{m}$

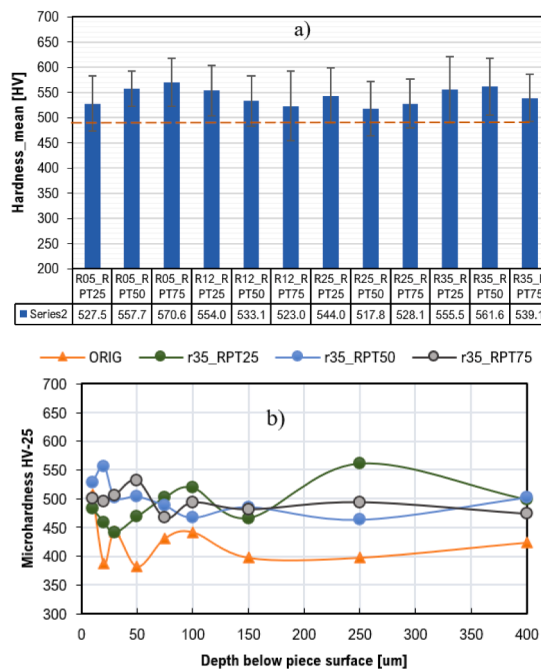
cutting edge radius, with normal and adequate winding according to the criteria established by ISO 3685:1993 for single-point turning tool life testing. When there is thermal influence during tool passage, deformation is induced in the primary zone of the cutting area. As a result, the entire chip is heated, friction decreases, and chip deformation occurs [46]. On the other hand, Fig. 16b illustrates the granular deformation that occurs in the surface layer of the workpiece as the tool passes through it. It is observed that the depth of granular involvement is around 40  $\mu\text{m}$  at the cutting conditions of  $RPT = 75 \mu\text{m}$  and  $r_\beta = 35 \mu\text{m}$ . This finding agrees with a similar observation made in the work of A. Sharman [47].

Fig. 17 shows the average surface quality,  $R_a$ , and the average roughness height,  $R_z$ , in both the cutting direction (Fig. 17a) and the cross direction (Fig. 17b) when cutting Inconel 718 under the experimental conditions. In addition, the 3D surface topography for the cutting conditions is shown for a maximum  $RPT$  of 75  $\mu\text{m}$  with the different radius. In general, it is observed that the surface roughness is better in the cutting direction, but different levels of swell are evidenced, which may be due to the damping effect on the cutting tool. When machining with a radius of 12  $\mu\text{m}$  the best roughness results are obtained in both longitudinal and cross directions. The 3D topographies in Fig. 17 show different surface roughness in the x-direction concerning the y-direction (cutting direction). This is because the topography obtained by machining in the cross direction is directly related to the loss of sharpness of the cutting edge.

Relating this to the tool edge wear shown in Fig. 12a, correspondence is observed between the level of cutting edge damage and the surface roughness results. In the cases of Fig. 12a and 12c, the trace of tool edge microcracks on the machined surface is reflected. Also, the level of surface swell is estimated to agree with the increase in edge radius in the cases of Fig. 12b and 12d, being lower in the machining with a radius of 12  $\mu\text{m}$ . As mentioned in the wear analysis, as the radius increases, the thrust force also increases, increasing the risk of the damping effect. However, this agreement between roughness and wear is not reflected in the surface hardness in the machined groove (Fig. 18). In all cases, the surface hardness increases compared to the pre-machining hardness, but the differences between the different cutting edge radii are insignificant. However, the microhardness below the machined surface evidence hardness increases in two depth bands below 100  $\mu\text{m}$  and around 200  $\mu\text{m}$  [47]. A further investigation of the hardness in the cutting zone and the study of the surface integrity will be carried out at a later stage.



**Fig. 17.** Average surface quality  $R_a$ , and average roughness height  $R_z$ , a) transverse cutting direction, b) cutting direction.



**Fig. 18.** Hardness, a) surface hardness in the different broached slots, b) microhardness profiles obtained at  $r_\beta$  35  $\mu\text{m}$  and different  $RPT$ .

#### 3.4. Temperature behavior on the tool cutting edge

The results of the temperature behavior as the tool passes are shown in Fig. 19. The temperatures shown correspond to the lateral area of the tool cutting edge (Fig. 19a). Fig. 19a shows that the temperature at the start of the cutting process rises and is maintained as the tool makes its way through the material, initiating the formation of the chip. Then, the temperature decreases by about 5 degrees as the chip formation stabilizes. This phenomenon is observed for all  $RPT$  values (Fig. 19b).

In addition, the effect of the cutting edge radius on the temperature in the machining process can be seen to be most significant when varying the  $RPT$ . The temperature tends to rise as the cutting edge radius increases, just as the temperature rises as the  $RPT$  increases. On the other hand, a particular effect on tool temperature was detected when using the smallest cutting edge radius. The temperatures are relatively high (Fig. 19b). This effect is estimated to be because the chip-tool contact length is longer when the edge radius is small. Therefore, there is more friction. This effect was also detected by García-González et al. [48] when machining Inconel 718. They state that the contact temperature is maximum at a finite distance from the cutting edge and smaller than the

contact length between the tool and the chip. The cutting radius in the García-González work was 2.5  $\mu\text{m}$ . On the other hand, increasing the cutting radius helps to reduce the temperature in the chip-tool interaction zone and distributes it along the cutting radius profile. This explanation can be given by performing FEM simulations of orthogonal cutting in the experimental conditions (Fig. 20).

#### 4. Conclusion

In this study, we analyzed the influence of cutting edge radius of roughing broaches on the machining of turbine disk fir trees tested in orthogonal broaching tests on Inconel 718 in dry conditions. We tested three cutting edge radii in combination with 4 Rise per tooth ( $RPT$ ) in the usual range of rough broaching to observe the behavior in cutting forces, tool temperature, specific cutting force, friction, and flank wear. The significant results are as follows:

- The cutting force components at broaching were similar, which may be due to form factors ( $RPT/r_\beta$ ) close to or less than 1, asymmetric wear on the cutting edge, and increased cutting edge radius.
- The shape factor ( $RPT/r_\beta$ ) could be the most influential in the increase of the cutting force components causing large plastic deformation, which was evident in the geometrical profile of the chips.
- The increase of the friction coefficients is influenced by the increase of the cutting edge radius the flank wear and the loss of sharpness of the cutting edge, reaching values of about 1.
- The change of cutting edge radius and  $RPT$  affects the tool temperature. Furthermore, the simulations allow to observe how the temperature concentration changes from a zone above the cutting edge to a distribution along the entire cutting edge radius profile.
- The cutting edge radius of 12  $\mu\text{m}$  has the best performance in terms of cutting force, temperature and surface quality.
- Polishing the cutting edge with ceramic bristle brushes is suitable for achieving a desired, symmetrical edge radius (K-factor close to 1). In addition, it improved the surface quality of the cutting edge by obtaining a roughness 2 to 3 times lower than the original value.
- In the future, monitoring data can help check the influence of tool micro geometry [3,49] and tool wear. Consequently, we intend to investigate further the effects on surface quality and changes in residual stresses and the application of special coatings on the tool that can be beneficial or counterproductive.

#### Funding

"This research was funded by the Ministry of Mineco Grant PID2019-109340RB-I00 and PDC2021-121792-I00 funded by MCIN/AEI/ <https://doi.org/10.13039/501100011033>. Thanks, are also due to European commission by H2020 project n. 958,357 InterQ Interlinked

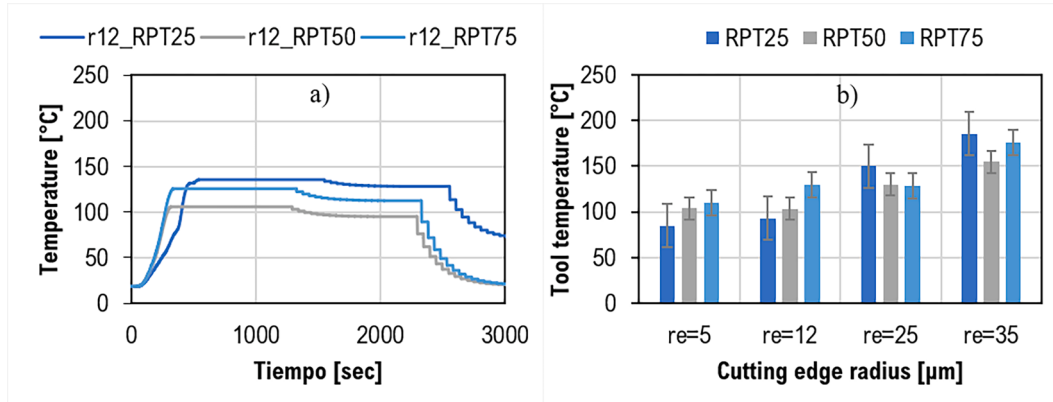


**Fig. 19.** Temperature behavior on the tool cutting edge, and a) 12  $\mu\text{m}$  radius broaching, (b) Temperature for all cutting conditions.

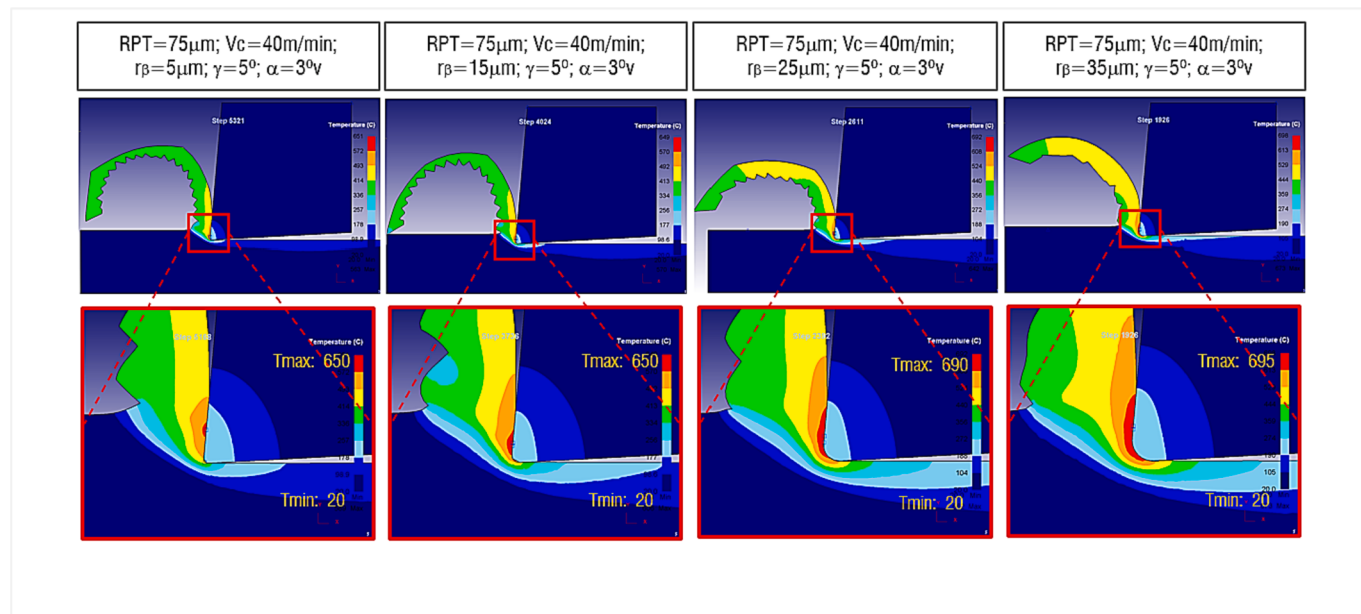


**Fig. 20.** Simulation of the temperature distribution in the chip-tool interaction zone for broaching Inconel 718 with RPT 75  $\mu\text{m}$  and for the different cutting edge radius tested.

Process, Product and Data Quality framework for Zero-Defects Manufacturing. Experiments were performed by help of project (QUOLINK TED2021-130044B-I00) Ministerio de Ciencia e Innovación 2021. In aspects related with modelling, support from the University Excellency groups grant by Basque Government IT 1573-22”.

#### Declaration of Competing Interest

The authors declare that they have no known competing financial interests or personal relationships that could have appeared to influence the work reported in this paper.

#### Acknowledgments

Thanks, are also given to special Unit AIMS, funded by the University of the Basque Country, Ideko, IMH and BCAM. We would like to thank the Universidad Técnica de Ambato for its support in the execution of the research. Thanks, are also due to G.Celaya from EKIN for the wise advice in CFAA broaching research projects.

#### References

- [1] S.P. Mo, D.A. Axinte, T.H. Hyde, N.N.Z. Gindy, An example of selection of the cutting conditions in broaching of heat-resistant alloys based on cutting forces, surface roughness and tool wear, *J. Mater. Process. Technol.* 160 (3) (2005) 382–389, <https://doi.org/10.1016/J.JMATPROTEC.2004.06.026>.
- [2] P.J. Arrazola, J. Rech, R. M'Saoubi, D. Axinte, Broaching: Cutting tools and machine tools for manufacturing high quality features in components, *CIRP Ann.* 69 (2) (2020) 554–577, <https://doi.org/10.1016/J.CIRP.2020.05.010>.
- [3] A. del Olmo, et al., Tool wear monitoring of high-speed broaching process with carbide tools to reduce production errors, *Mech. Syst. Sig. Process.* 172 (2022), 109003, <https://doi.org/10.1016/J.YMSSP.2022.109003>.
- [4] P. Vogtel, F. Klocke, D. Lung, S. Terzi, Automatic Broaching Tool Design by Technological and Geometrical Optimization, *Procedia CIRP* 33 (2015) 496–501, <https://doi.org/10.1016/j.procir.2015.06.061>.
- [5] F. Zanger, N. Boev, V. Schulze, Surface Quality after Broaching with Variable Cutting Thickness, *Procedia CIRP* 13 (2014) 114–119, <https://doi.org/10.1016/j.procir.2014.04.020>.
- [6] P. Vogtel, F. Klocke, H. Puls, S. Buchkremer, D. Lung, Modelling of process forces in broaching Inconel 718, *Procedia CIRP* 8 (2013) 409–414, <https://doi.org/10.1016/j.procir.2013.06.125>.
- [7] V. Schulze, N. Boev, F. Zanger, Numerical Investigation of the Changing Cutting Force Caused by the Effects of Process Machine Interaction While Broaching, *Procedia CIRP* 4 (2012) 140–145, <https://doi.org/10.1016/j.procir.2012.10.025>.
- [8] D. Fabre, C. Bonnet, J. Rech, T. Mabrouki, Optimization of surface roughness in broaching, *CIRP J. Manuf. Sci. Technol.* 18 (2017) 115–127, <https://doi.org/10.1016/J.CIRPJ.2016.10.006>.
- [9] W. Grzesik, P. Niesłony, W. Habrat, J. Sieniawski, P. Laskowski, Investigation of tool wear in the turning of Inconel 718 superalloy in terms of process performance and productivity enhancement, *Tribol. Int.* 118 (2018) 337–346, <https://doi.org/10.1016/J.TRIPOINT.2017.10.005>.
- [10] P.J. Arrazola, D. Ugarte, X. Dominguez, A new approach for the friction identification during machining through the use of finite element modeling, *Int J Mach Tool Manu* 48 (2) (2008) 173–183, <https://doi.org/10.1016/j.ijmachtools.2007.08.022>.
- [11] K.D. Bouzakis, et al., Effect of cutting edge preparation of coated tools on their performance in milling various materials, *CIRP J. Manuf. Sci. Technol.* 7 (3) (2014) 264–273, <https://doi.org/10.1016/J.CIRPJ.2014.05.003>.
- [12] A.I. Fernández-Abia, J. Barreiro, L.N. López de Lacalle, S. Martínez-Pellitero, Behavior of austenitic stainless steels at high speed turning using specific force coefficients, *Int. J. Adv. Manuf. Technol.* 62 (5–8) (2012) 505–515, <https://doi.org/10.1007/s00170-011-3846-9>.
- [13] S. Rodríguez-Barrero, J. Fernández-Larrinoa, I. Azkona, L.N. López de Lacalle, R. Polvorosa, Enhanced Performance of Nanostructured Coatings for Drilling by Droplet Elimination, *Mater. Manuf. Process.* 31 (5) (2016) 593–602, <https://doi.org/10.1080/10426914.2014.973582>.
- [14] Y. Alammari, I. Iovkov, J. Saelzer, T. Wolf, D. Biermann, Adhesion of Inconel 718 on Uncoated Tungsten Carbide Inserts in Interrupted Orthogonal Machining under MQL, *Procedia CIRP* 103 (2021) 194–199, <https://doi.org/10.1016/J.PROCIR.2021.10.031>.
- [15] D. Ulutan, T. Öznel, Determination of tool friction in presence of flank wear and stress distribution based validation using finite element simulations in machining of titanium and nickel based alloys, *J. Mater. Process. Technol.* 213 (12) (2013) 2217–2237, <https://doi.org/10.1016/J.JMATPROTEC.2013.05.019>.
- [16] E. Park, D.M. Kim, H.W. Park, Y. Bin Park, N. Kim, Evaluation of Tool Life in the Dry Machining of Inconel 718 Parts from Additive Manufacturing (AM), *Int. J. Precis. Eng. Manuf.* 21 (1) (2020) 57–65, <https://doi.org/10.1007/S12541-019-00275-X/FIGURES/9>.
- [17] H. Puls, F. Klocke, D. Lung, A new experimental methodology to analyse the friction behaviour at the tool-chip interface in metal cutting, *Prod. Eng.* 6 (4–5) (2012) 349–354, <https://doi.org/10.1007/s11740-012-0386-6>.
- [18] B. Peng, T. Bergs, D. Schraknepper, T. Smigielski, F. Klocke, Development and validation of a new friction model for cutting processes, *Int. J. Adv. Manuf. Technol.* 107 (11–12) (2020) 4357–4369, <https://doi.org/10.1007/s00170-019-04709-8>.
- [19] H. Saglam, F. Unsacar, S. Yaldiriz, Investigation of the effect of rake angle and approaching angle on main cutting force and tool tip temperature, *Int J Mach Tool Manu* 46 (2) (2006) 132–141, <https://doi.org/10.1016/j.ijmachtools.2005.05.002>.
- [20] P. Li, Z. Chang, Numerical Modeling of the Effect of Cutting-Edge Radius on Cutting Force and Stress Concentration during Machining, *Micromachines (basel)* 13 (2) (2022) 211, <https://doi.org/10.3390/mi13020211>.
- [21] T.H.C. Childs, K. Maekawa, T. Obikawa, *Metal machining: theory and applications*, Butterworth-Heinemann, 2000.
- [22] S.P.F.C. Jaspers, *Metal cutting mechanics and material behaviour*, Eindhoven University of Technology, 1999.

- [23] N.N. Zorev, Inter-relationship between shear processes occurring along tool face and shear plane in metal cutting, *International Research in Production Engineering* 49 (1963) 143–152.
- [24] W. Grzesik, Experimental investigation of the influence of adhesion on the frictional conditions in the cutting process, *Tribol. Int.* 32 (1) (1999) 15–23, [https://doi.org/10.1016/S0301-679X\(99\)00004-3](https://doi.org/10.1016/S0301-679X(99)00004-3).
- [25] N. Fang, P.S. Pai, S. Mosquea, Effect of tool edge wear on the cutting forces and vibrations in high-speed finish machining of Inconel 718: an experimental study and wavelet transform analysis, *Int. J. Adv. Manuf. Technol.* 52 (1–4) (2011) 65–77, <https://doi.org/10.1007/s00170-010-2703-6>.
- [26] B. Denkena, J. Köhler, C.E.H. Ventura, Customized cutting edge preparation by means of grinding, *Precis. Eng.* 37 (3) (2013) 590–598, <https://doi.org/10.1016/J.PRECISIONENG.2013.01.004>.
- [27] E. Díaz-Tena, U. Ugalde, L.N. López de Lacalle, A. de la Iglesia, A. Calleja, F. J. Campa, Propagation of assembly errors in multitasking machines by the homogenous matrix method, *Int. J. Adv. Manuf. Technol.* 68 (1–4) (2013) 149–164, <https://doi.org/10.1007/s00170-012-4715-x>.
- [28] P. Klocek, “Handbook of infrared optical materials,” *Handbook of Infrared Optical Materials*, pp. 1–611, 2017, doi: 10.1201/9781315213996.
- [29] ASTM, “E1933-14 Standard Practice for Measuring and Compensating for Emissivity Using Infrared Imaging Radiometers.” Accessed: May 05, 2023. [Online]. Available: <https://www.astm.org/e1933-14r18.html>.
- [30] N.N. Zorev, *Interrelationship between Shear Processes Occurring along Tool Faces and on Shear Plane in Metal Cutting*, in: *Proceedings of the International Production Engineering Research Conference, ASME, New York, 1963*, pp. 42–49.
- [31] M. Eugene Merchant, “Basic Mechanics of the Metal-Cutting Process,” *J Appl Mech*, vol. 11, no. 3, pp. A168–A175, 1944, doi: 10.1115/1.4009380.
- [32] P. Albrecht, New Developments in the Theory of the Metal-Cutting Process: Part I. The Ploughing Process in Metal Cutting, *J. Eng. Ind.* 82 (4) (1960) 348–357, <https://doi.org/10.1115/1.3664242>.
- [33] Tom. Drozda, Charles. Wick, J. T. Benedict, R. F. Veilleux, Ramon. Bakerjian, and Society of Manufacturing Engineers., “Tool and Manufacturing Engineers Handbook; Volume I: Machining,” vol. I, pp. 1–1494, 1983.
- [34] Y.L. Zhang, W.Y. Chen, Finite Element Modeling of the Broaching Process of Inconel718, *Mater. Sci. Forum* 697–698 (2012) 39–43, <https://doi.org/10.4028/WWW.SCIENTIFIC.NET/MSF.697-698.39>.
- [35] C.F. Wyen, K. Wegener, Influence of cutting edge radius on cutting forces in machining titanium, *CIRP Ann.* 59 (1) (2010) 93–96, <https://doi.org/10.1016/J.CIRP.2010.03.056>.
- [36] D.A. Lucca, Y.W. Seo, R. Komanduri, Effect of Tool Edge Geometry on Energy Dissipation in Ultraprecision Machining, *CIRP Ann.* 42 (1) (1993) 83–86, [https://doi.org/10.1016/S0007-8506\(07\)62397-X](https://doi.org/10.1016/S0007-8506(07)62397-X).
- [37] M.A. Rahman, M. Rahman, M. Mia, M.K. Gupta, B. Sen, A. Ahmed, Investigation of the specific cutting energy and its effect in shearing dominant precision micro cutting, *J. Mater. Process. Technol.* 283 (2020), 116688, <https://doi.org/10.1016/J.JMATPROTEC.2020.116688>.
- [38] X. Sun and K. Cheng, “Micro-/Nano-Machining through Mechanical Cutting,” *Micromanufacturing Engineering and Technology*, pp. 24–38, 2010, doi: 10.1016/B978-0-8155-1545-6.00002-8.
- [39] G. Xiong, J. Liu, and A. Avila, “Cutting tool wear measurement by using active contour model based image processing,” *2011 IEEE International Conference on Mechatronics and Automation, ICMA 2011*, pp. 670–675, 2011, doi: 10.1109/ICMA.2011.5985741.
- [40] W.H. Wang, G.S. Hong, Y.S. Wong, Flank wear measurement by a threshold independent method with sub-pixel accuracy, *Int J Mach Tool Manu* 46 (2) (2006) 199–207, <https://doi.org/10.1016/J.IJMACHTOOLS.2005.04.006>.
- [41] J. Loizou, W. Tian, J. Robertson, J. Camelio, Automated wear characterization for broaching tools based on machine vision systems, *J. Manuf. Syst.* 37 (2015) 558–563, <https://doi.org/10.1016/J.JMYS.2015.04.005>.
- [42] I. Holgado, C. Pérez-Salinas, N. Ortega, L. N. López de Lacalle, and A. Del Olmo, “An intelligent machine learning based method for tool wear estimation in the vertical broaching process,” Springer Nature, XV Iberoamerican Congress of Mechanical Engineering, pp. 251–57, 2023, doi: 10.1007/978-981-13-6447-1\_70/FIGURES/.
- [43] R.N. Roth, P.L.B. Oxley, Slip-Line Field Analysis for Orthogonal Machining Based upon Experimental Flow Fields, *J. Mech. Eng. Sci.* 14 (2) (1972) 85–97, [https://doi.org/10.1243/JMES\\_JOUR\\_1972\\_014\\_015\\_02](https://doi.org/10.1243/JMES_JOUR_1972_014_015_02).
- [44] A. Uysal, E. Altan, A New Slip-Line Field Modeling of Orthogonal Machining with a Rounded-Edge Wear Cutting Tool, *Mach. Sci. Technol.* 18 (3) (2014) 386–423, <https://doi.org/10.1080/10910344.2014.925375>.
- [45] A.K. Parida, K. Maity, Effect of nose radius on forces, and process parameters in hot machining of Inconel 718 using finite element analysis, *Eng. Sci. Technol., Int. J.* 20 (2) (2017) 687–693, <https://doi.org/10.1016/j.jestch.2016.10.006>.
- [46] V. Schulze, H. Meier, T. Strauss, J. Gibmeier, High Speed Broaching of Case Hardening Steel SAE 5120, *Procedia CIRP* 1 (2012) 431–436, <https://doi.org/10.1016/j.procir.2012.04.077>.
- [47] A.R.C. Sharman, J.I. Hughes, K. Ridgway, Surface integrity and tool life when turning Inconel 718 using ultra-high pressure and flood coolant systems, *Proc. Inst. Mech. Eng. B J. Eng. Manuf.* 222 (6) (2008) 653–664, <https://doi.org/10.1243/09544054JEM936>.
- [48] J.C. Garcia-Gonzalez, W. Moscoso-Kingsley, V. Madhavan, Tool Rake Face Temperature Distribution When Machining Ti6Al4V and Inconel 718, *Procedia Manuf.* 5 (2016) 1369–1381, <https://doi.org/10.1016/J.PROMFG.2016.08.107>.
- [49] D.A. Axinte, N. Gindy, Tool condition monitoring in broaching, *Wear* 254 (3–4) (2003) 370–382, [https://doi.org/10.1016/S0043-1648\(03\)00003-6](https://doi.org/10.1016/S0043-1648(03)00003-6).